Control of a quantum emitter's bandwidth by managing its reactive power

Iñigo Liberal,[1,2] Iñigo Ederra,[1,2] and Richard W. Ziolkowski[3]

[1]*Electrical and Electronic Engineering Department, Universidad Pública de Navarra, Campus Arrosadía, Pamplona 31006, Spain*

[2]*Institute of Smart Cities, Universidad Pública de Navarra, Campus Arrosadía, Pamplona 31006, Spain*

[3]*Global Big Data Technologies Centre, University of Technology Sydney, Ultimo, NSW 2007, Australia*

(Received 24 August 2018; published 20 August 2019)

Reactive power plays a crucial role in the design of small antenna systems, but its impact on the bandwidth of quantum emitters is typically disregarded. Here, we theoretically demonstrate that there is an intermediate domain between the usual weak- and strong-coupling regimes where the bandwidth of a quantum emitter is directly related to the dispersion properties of the reactive power. This result emphasizes that reactive power must be understood as an additional degree of freedom in engineering the bandwidth of quantum emitters. We illustrate the applicability of this concept by revisiting typical configurations of quantum emitters coupled to resonant cavities and waveguides. Analysis of the reactive power in these systems unveils functionalities including the design of efficient but narrow-band photon sources, as well as quantum emitters exhibiting bandwidths narrower than their nonradiative linewidths even under incoherent pumping.

DOI: 10.1103/PhysRevA.100.023830

I. INTRODUCTION

The analysis of reactive power [1,2] and related quantities such as stored energy [3,4] plays a central role in the design of classical radiating systems and the identification of their fundamental limits. This aspect is particularly relevant for electrically small antennas, since the smaller the size of an emitter the larger the impact of the reactive fields on its performance. In fact, following the pioneering works of Wheeler [5], Chu [6], and Harrington [7], much attention has been devoted to the analysis of stored energy and the derivation of physical bounds of antenna performance [8–15] (see, e.g., [16] for a historical review). The importance of these works is that they fundamentally establish what is possible and what is not possible to do with an antenna system. They also inspire different antenna designs that approach the theoretical limits [17–20] and facilitate the implementation of optimization procedures [21–23].

In contrast, the concept of reactive power is strange to the field of quantum optics and the design of quantum emitters. Although interactions with so-called virtual photons are considered (see, e.g., the recent perspective [24]), these primarily lead to shifts of the emission frequency [see Figs. 1(a) and 1(b)]. Different versions of these shifts include the celebrated Lamb shift [25], collective Lamb shift [26,27], and medium-assisted shifts [28–30]. In general, the spectrum is Lorentzian and its linewidth is determined by the decay rate [see Fig. 1(b)]. Therefore, it appears that the interaction with virtual photons and/or reactive fields has no impact on the bandwidth of a quantum emitter. This point might appear to be particularly surprising since most quantum emitters are deeply subwavelength radiators, even more so than electrically small antennas.

At the same time, it is known that this behavior relates to the operation within the weak-coupling regime. On the other hand, when a small quantum system is strongly coupled to a photonic nanostructure, their interactions through the radiation field can significantly impact its emission spectrum. One particularly popular example is the vacuum Rabi splitting, where the strong interaction between the emitter and a cavity mode results in a two-peaked spectrum (see, e.g., [31]). Therefore, it is clear that when the coupling is sufficiently strong the energy stored in the radiation field must have an impact on the bandwidth of a quantum emitter. Different works have addressed the emission spectrum of a quantum emitter in the weak- and strong-coupling regimes [32–36]. However, the role of reactive interactions on the bandwidth of a quantum emitter, and the possibilities that could be accessed by engineering it, have not yet been explored. The emission spectrum can also be modified via collective interactions with other emitters, e.g., super-radiance, sub-radiance, or collective Lamb shift effects. However, these approaches typically require a means to preserve the coherent interactions between several, usually identical, emitters, which is more challenging from an experimental point of view. As a consequence, they will not be considered herein.

Here, we theoretically investigate the bandwidth of a quantum emitter amid its transition from the weak- to the strong-coupling regime, emphasizing the role of the reactive power associated with the emitter's current distribution. Specifically, we demonstrate that there is an intermediate domain between the usual weak- and strong-coupling regimes in which the emission spectrum is Lorentzian, but the associated bandwidth of the emitters is directly affected by the dispersion properties of the reactive power [see Fig. 1(c)]. This result highlights the reactive power as an additional degree of freedom in controlling the quantum emitter's bandwidth that can be harnessed to introduce photon sources with unprecedented characteristics. Specifically, we will demonstrate how managing the reactive power enables (i) increasing the efficiency of a quantum emitter while maintaining a narrow bandwidth and (ii) designing a quantum emitter exhibiting a bandwidth

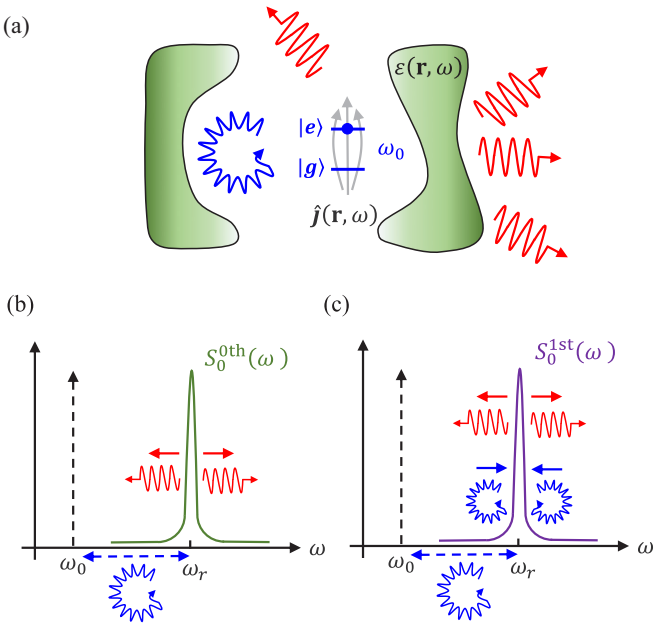

FIG. 1. (a) Sketch of the general configuration: A quantum emitter, modeled as a two-level system $\{|e\rangle, |g\rangle\}$ with a transition frequency ω_0, has an effective current distribution $\widehat{\mathbf{j}}(\mathbf{r},\omega)$ that is coupled to a photonic environment characterized by a relative permittivity $\varepsilon(\mathbf{r},\omega)$. (b) Zeroth-order (weak-coupling) approximation to the emission spectrum, where reactive interactions shift the emission frequency from ω_0 to ω_r and radiative interactions define its bandwidth. (c) First-order correction to the spectrum where both radiative and reactive interactions impact the emission bandwidth.

narrower than its nonradiative linewidth, even with incoherent excitation.

II. THEORETICAL FRAMEWORK

As schematically depicted in Fig. 1, we investigate the emission properties of a small quantum system modeled as a two-level system. It has excited $|e\rangle = \int d^3\mathbf{r}\, \psi_e(\mathbf{r})|\mathbf{r}\rangle$ and ground $|g\rangle = \int d^3\mathbf{r}\, \psi_g(\mathbf{r})|\mathbf{r}\rangle$ states that are separated by the transition frequency ω_0. The system is coupled to a macroscopic lossy photonic environment that is characterized by the dispersive relative permittivity $\varepsilon(\mathbf{r},\omega) = \varepsilon_R(\mathbf{r},\omega) + i\,\varepsilon_I(\mathbf{r},\omega)$. We model this quantum system within the framework of macroscopic QED (see, e.g., [35]). Its Hamiltonian can be written as

$$\widehat{H} = \widehat{H}_0 + \widehat{H}_B + \widehat{H}_I, \tag{1}$$

with

$$\widehat{H}_0 = \frac{\hbar\omega_0}{2}\,\widehat{\sigma}_z, \tag{2}$$

$$\widehat{H}_B = \int_0^\infty d\omega_f \int d^3\mathbf{r}\, \hbar\omega_f\, \widehat{\mathbf{f}}^\dagger(\mathbf{r},\omega_f)\cdot\widehat{\mathbf{f}}(\mathbf{r},\omega_f), \tag{3}$$

$$\widehat{H}_I = -\frac{q}{2m}\left[\widehat{\mathbf{p}}\cdot\widehat{\mathbf{A}}(\widehat{\mathbf{r}}) + \widehat{\mathbf{A}}(\widehat{\mathbf{r}})\cdot\widehat{\mathbf{p}}\right] + \frac{q^2}{2m}\widehat{\mathbf{A}}^2(\widehat{\mathbf{r}}), \tag{4}$$

where $\widehat{\mathbf{r}}$ and $\widehat{\mathbf{p}}$ are the position and momentum operators, respectively; m is the mass of the electron; and $\widehat{\sigma}_z = |e\rangle\langle e| - |g\rangle\langle g|$ and $\widehat{\mathbf{f}}(\mathbf{r},\omega_f)$ are polaritonic operators representing the excitations of the photonic environment. The vector potential operator is given by

$$\widehat{\mathbf{A}}(\mathbf{r}) = \int_0^\infty d\omega_f \int d^3\mathbf{r}' \sqrt{\frac{\hbar}{\pi\varepsilon_0}}\frac{\omega_f}{c^2}\sqrt{\varepsilon_I(\mathbf{r}',\omega_f)} \times\{\mathbf{G}(\mathbf{r},\mathbf{r}',\omega_f)\cdot\widehat{\mathbf{f}}(\mathbf{r}',\omega_f) + \text{H.c.}\}, \tag{5}$$

where $\mathbf{G}(\mathbf{r},\mathbf{r}',\omega_f)$ is the dyadic Green's function of the macroscopic environment.

In order to draw a closer connection with classical antenna theory, we rewrite the interaction Hamiltonian as a function of a current density operator. To this end, we disregard the $\widehat{\mathbf{A}}^2(\mathbf{r})$ nonlinear term and expand the vector potential operator in the position representation to find that the interaction Hamiltonian can be rewritten as follows:

$$\widehat{H}_I = -\int d^3\mathbf{r}\,\widehat{\mathbf{j}}(\mathbf{r})\cdot\widehat{\mathbf{A}}(\mathbf{r}). \tag{6}$$

Here, we have defined the current density operator

$$\widehat{\mathbf{j}}(\mathbf{r}) = \frac{1}{2m}\,\widehat{\rho}(\mathbf{r})\widehat{\mathbf{p}} + \text{H.c.}, \tag{7}$$

where $\widehat{\rho}(\mathbf{r}) = q|\mathbf{r}\rangle\langle\mathbf{r}|$. These operators are defined such that their expectation values recover the charge density $\rho(\mathbf{r},t) = \langle\widehat{\rho}(\mathbf{r})\rangle = q|\psi(\mathbf{r},t)|^2$ and the current density $\mathbf{j}(\mathbf{r},t) = \langle\widehat{\mathbf{j}}(\mathbf{r})\rangle = \frac{q}{2m}(-i\hbar)\psi^*(\mathbf{r},t)\nabla\psi(\mathbf{r},t) + \text{H.c.}$, in such a manner that they satisfy the continuity equation $\partial_t\rho(\mathbf{r},t) + \nabla\cdot\mathbf{j}(\mathbf{r},t) = 0$ (see, e.g., [37] p. 32). For a two-level system, $\{|e\rangle, |g\rangle\}$, the current density operator can be decomposed as follows: $\widehat{\mathbf{j}}(\mathbf{r}) = \mathbf{j}_{ge}(\mathbf{r})\widehat{\sigma} + \mathbf{j}_{ge}^*(\mathbf{r})\widehat{\sigma}^\dagger + \mathbf{j}_{ee}(\mathbf{r})\widehat{\sigma}^\dagger\widehat{\sigma} + \mathbf{j}_{gg}(\mathbf{r})\widehat{\sigma}\widehat{\sigma}^\dagger$, with $\mathbf{j}_{ab}(\mathbf{r}) = \langle a|\widehat{\mathbf{j}}(\mathbf{r})|b\rangle$ and $\widehat{\sigma} = |g\rangle\langle e|$.

In the following, we will be mostly concerned with the properties of the fields generated by the quantum emitters. Therefore, we compute the source field operators in the Heisenberg picture by solving the equation of motion, $i\hbar\,\partial_t\widehat{a} = [\widehat{a},\widehat{H}]$, for the polaritonic operator $\widehat{\mathbf{f}}(\mathbf{r}',\omega_f;t)$, and we find that the Laplace transform of the source vector potential and electric-field operator can be conveniently written in analogy with their classical counterparts as functions of the current density as follows:

$$\widehat{\mathbf{A}}_S(\mathbf{r};\omega) = \mu_0\int d^3\mathbf{r}'\,\mathbf{G}(\mathbf{r},\mathbf{r}',\omega)\cdot\widehat{\mathbf{j}}(\mathbf{r}',\omega), \tag{8}$$

$$\widehat{\mathbf{E}}_S(\mathbf{r};\omega) = i\omega\mu_0\int d^3\mathbf{r}'\,\mathbf{G}(\mathbf{r},\mathbf{r}',\omega)\cdot\widehat{\mathbf{j}}(\mathbf{r}',\omega). \tag{9}$$

III. EMISSION SPECTRUM

Next we examine the emission spectrum during a decay process, i.e., when the emitter is initially excited and the photonic environment is in its vacuum state: $|\psi(t=0)\rangle = |e\rangle|\{0\}\rangle$. This configuration is relevant for incoherent pumping or when the quantum emitter is resonantly excited via an initialization pulse. Similar to the usual rotating wave approximation, we approximate the interaction Hamiltonian by keeping only those terms that preserve the number of excitations:

$$\widehat{H}_I = -\int d^3\mathbf{r}\,(\widehat{\sigma}^\dagger(t)\,\mathbf{j}_{\text{ge}}^*(\mathbf{r})\cdot\widehat{\mathbf{A}}_S^{(+)}(\mathbf{r};t) + \text{H.c.}), \tag{10}$$

where $\widehat{\mathbf{A}}_S^{(+)}(\mathbf{r};t)$ is the inverse Laplace transform of $\widehat{\mathbf{A}}_S^{(+)}(\mathbf{r};\omega) = \mu_0 \int d^3\mathbf{r}'\, \mathbf{G}(\mathbf{r},\mathbf{r}',\omega)\cdot\mathbf{j}_{\rm ge}(\mathbf{r}')\widehat{\sigma}(\omega)$. Adapting the theory introduced in [32–34,36] to our current density formulation within the one-photon correlation approximation, we find that the emission spectrum is given by

$$\begin{aligned} S(\mathbf{r},\omega) &= \langle (\widehat{\mathbf{E}}_S^{(+)}(\mathbf{r};\omega))^\dagger \cdot \widehat{\mathbf{E}}_S^{(+)}(\mathbf{r};\omega)\rangle \\ &= C_{\rm prop}(\mathbf{r},\omega) S_0(\omega), \end{aligned} \tag{11}$$

with

$$C_{\rm prop}(\mathbf{r},\omega) = \omega^2\mu_0^2 \left| \int d^3\mathbf{r}'\, \mathbf{G}(\mathbf{r},\mathbf{r}',\omega)\cdot\mathbf{j}_{\rm ge}(\mathbf{r}') \right|^2 \tag{12}$$

being the propagation term which accounts for the directive emission properties of the current density and its environment. The term $S_0(\omega) = \langle \widehat{\sigma}^\dagger(\omega)\widehat{\sigma}(\omega)\rangle$ is the polarization spectrum; it accounts for the impact of the emitter dynamics. It can be written as

$$S_0(\omega) = \frac{1}{[\omega - \omega_0 - \Delta\omega(\omega)]^2 + \frac{\Gamma^2(\omega)}{4}}. \tag{13}$$

We have defined in this expression the (in general, dispersive) decay rate, $\Gamma(\omega)$, and frequency shift, $\Delta\omega(\omega)$, which can be written as a function of the current densities as follows:

$$\begin{aligned} &\Delta\omega(\omega) - i\,\frac{\Gamma(\omega}{2} \\ &\quad = -\frac{\mu_0}{\hbar}\int d^3\mathbf{r} \int d^3\mathbf{r}'\, \mathbf{j}_{\rm ge}^*(\mathbf{r})\cdot\mathbf{G}(\mathbf{r},\mathbf{r}',\omega)\cdot\mathbf{j}_{\rm ge}(\mathbf{r}'). \end{aligned} \tag{14}$$

In view of Eq. (14), it is elucidating to draw an analogy with classical antenna theory. In fact, although the expressions for $\Gamma(\omega)$ and $\Delta\omega(\omega)$ have been derived within the macroscopic QED formalism in a self-consistent manner, they present a clear mathematical analogy with the fields radiated by a classical current density $\mathbf{j}_{\rm ge}(\mathbf{r})$. In order to illustrate this point, we define $\mathbf{E}_{cl}(\mathbf{r},\omega) = i\omega\mu_0 \int d^3\mathbf{r}'\, \mathbf{G}(\mathbf{r},\mathbf{r}',\omega)\cdot\mathbf{j}_{\rm ge}(\mathbf{r}')$ as the classical time-harmonic field [$\exp(-i\omega t)$ time convention] that would be generated by the current distribution $\mathbf{j}_{\rm ge}(\mathbf{r}')$. In doing so, we can directly relate the dispersive decay rate and frequency shift to the supplied and reactive powers associated with this classical current density, respectively [1,2]:

$$\Delta\omega(\omega) - i\,\frac{\Gamma(\omega)}{2} = \frac{2}{\hbar\omega}\,[P_{\rm reac}(\omega) - iP_{\rm sup}(\omega)], \tag{15}$$

with

$$P_{\rm sup} = \frac{1}{2}\oint_{S_\infty} d\mathbf{S}\cdot(\mathbf{E}_{\rm cl}\times\mathbf{H}_{\rm cl}^*) + \frac{\omega}{2}\int_{V_\infty} d^3\mathbf{r}\,\varepsilon_0\,\varepsilon_I(\mathbf{r},\omega)|\mathbf{E}_{\rm cl}|^2 \tag{16}$$

and

$$P_{\rm reac} = \frac{\omega}{2}\int_{V_\infty} d^3\mathbf{r}\,[\varepsilon_0\,\varepsilon_R(\mathbf{r},\omega)|\mathbf{E}_{\rm cl}|^2 - \mu_0|\mathbf{H}_{\rm cl}|^2]. \tag{17}$$

The volume integrals are taken over an asymptotically large volume, V_∞, bounded by a surface S_∞ in the far zone of the sources $\mathbf{j}_{\rm ge}(\mathbf{r})$. On the one hand, $P_{\rm sup}$ is the time-averaged power supplied by the current distribution $\mathbf{j}_{\rm ge}(\mathbf{r})$. It contains both the power radiated away from the system as well as the power dissipated in the surrounding environment. The reactive power, $P_{\rm reac}$, is related to the energy stored in the electric and magnetic fields during the interaction process; but it does not lead to any net energy transfer. However, it has a critical impact on the performance of classical systems, including its bandwidth and robustness against undesired loss channels, as well as stability and linearity aspects. Therefore, it could be expected that reactive interactions should also play a role in the performance of a quantum emitter, beyond determining its frequency of operation.

In general, it is clear from Eq. (13) that the polarization emission spectrum for a quantum emitter is determined by the dispersion properties of $\Delta\omega(\omega)$ and $\Gamma(\omega)$. We can expect that the spectrum will exhibit peaks at the resonant frequencies given by the solutions to the implicit equation $\omega_r = \omega_0 + \Delta\omega(\omega_r)$. In the neighborhood of one of these resonances, the zeroth-order approximation to the emission spectrum would be to neglect all dispersion properties near the resonance frequency. This approximation recovers the usual Born-Markov approximation (or weak-coupling regime), which leads to the zeroth-order (Lorentzian) spectrum depicted in Fig. 1(b):

$$S_0^{\rm zeroth}(\omega) = \frac{1}{(\omega-\omega_r)^2 + \frac{\Gamma^2(\omega_r)}{4}}. \tag{18}$$

Within this approximation, the 3-dB bandwidth of the emission (frequency range between the half-maximum points) will be simply given by the decay rate $BW_{3\,\rm dB}^{\rm zeroth} = \Gamma(\omega_r)$. In stark contrast with antenna theory, while the reactive part of the interaction energy term is intimately related to the stored energy, it does not have any impact on the quantum emitter's bandwidth. As anticipated at the outset, this feature is in part surprising since quantum emitters are deeply subwavelength structures. Intuitively, the reason for this behavior is that, in contrast with small antennas, the quantum emitter is already intrinsically tuned to the resonance and the interaction with the electromagnetic field is considered a small perturbation. Therefore, the reactive energy term only leads to a small perturbative frequency shift.

However, this behavior changes when the strength of the coupling to the photonic environment is increased and leads to significant changes on the emission spectrum. In order to elucidate the transition between the usual weak- and strong-coupling regimes, we next introduce a first-order correction to the emission spectrum. To this end, we take a Taylor series expansion of $\Delta\omega(\omega)$ around ω_r. We also note in analogy with resonant antennas [4] that quantum emitters are typically tuned to be at either a maximum or a minimum of the dispersive decay rate, i.e., at a frequency for which $\partial_\omega\Gamma(\omega_r) \simeq 0$. The specific choice depends on whether one is using a photonic nanostructure to accelerate or decelerate the spontaneous emission process. Admittedly, there are other scenarios in which the dispersion properties of the decay rate cannot be neglected or can even be dominant. As shown in Appendix A, this mainly leads to an asymmetric Lorentzian line.

Here, we are mainly interested in the impact of reactive interactions on the emission spectrum, and their ability to control the emission bandwidth. Therefore, we introduce a first-order correction to the emission spectrum by approximating $\Delta\omega(\omega) \simeq \Delta\omega(\omega_r) + (\omega-\omega_r)\partial_\omega\Delta\omega(\omega_r)$ and $\Gamma(\omega) \simeq \Gamma(\omega_r)$. This approximation leads to the following first-order

correction to the emission spectrum:

$$S_0^{\text{first}}(\omega) = A\,\frac{1}{(\omega-\omega_r)^2+\frac{1}{4}\left(\frac{\Gamma(\omega_r)}{1-\partial_\omega\triangle\omega(\omega_r)}\right)^2}, \tag{19}$$

with $A=[1-\partial_\omega\triangle\omega(\omega_r)]^{-2}$. It is clear from Eq. (19) that the emission spectrum still preserves a Lorentzian line shape within this first-order correction. However, the linewidth is not entirely determined by the decay rate, but it directly depends on the dispersion of the frequency shift, $BW_{3\,\text{dB}}^{\text{first}}=\Gamma(\omega_r)/[1-\partial_\omega\triangle\omega(\omega_r)]$. This implies that one has an additional degree of freedom to control the bandwidth of the quantum emitter, opening new possibilities in the design of a quantum emitter's bandwidth [see Fig. 1(c)].

In order to understand what is possible and what is not possible to do with this extra degree of freedom, it is interesting to further draw analogies with classical antenna theory. In particular, the dispersion properties of the frequency shift, $\partial_\omega\triangle\omega(\omega)=\partial_\omega\{2\omega^{-1}P_{\text{reac}}(\omega)\}$, are directly related to the dispersion of the reactive power, i.e., $\partial_\omega P_{\text{reac}}(\omega)$. Adapting the derivations in [1,4] to our purposes, the latter can be written in terms of field related quantities as follows (see Appendix B):

$$\begin{aligned}\partial_\omega P_{\text{reac}} = &-\frac{1}{2}\int_{V_\infty} d^3\mathbf{r}\,[\mu_0|\mathbf{H}_{\text{cl}}|^2+\varepsilon_0\,\partial_\omega\{\omega\varepsilon_R(\mathbf{r},\omega)\}|\mathbf{E}_{\text{cl}}|^2]\\ &+\omega\,\varepsilon_0\int_{V_\infty} d^3\mathbf{r}\;\varepsilon_I(\mathbf{r},\omega)\text{Im}\left\{\mathbf{E}_{\text{cl}}^*\cdot\partial_\omega\mathbf{E}_{\text{cl}}\right\}\\ &+\mu_0\oint_{S_\infty} d\Omega\, r|\mathbf{F}(\mathbf{u}_r,\omega)|^2,\end{aligned} \tag{20}$$

where $\mathbf{F}(\mathbf{u}_r,\omega)$ is the emission pattern in the far zone, i.e., in the limit $\lim_{r\to\infty}\mathbf{E}_{\text{cl}}(\mathbf{r},\omega)=(e^{i\frac{\omega}{c}r}/r)\,\mathbf{F}(\mathbf{u}_r,\omega)$.

Equation (20) provides information about the behavior of the system in some limiting cases. For example, if the system can be considered lossless, i.e., when $\varepsilon_I(\mathbf{r},\omega_r)\to 0$, and nonradiating, i.e., when $\mathbf{F}(\mathbf{u}_r,\omega_r)\to 0$ near the resonant frequency ω_r, we can write $\partial_\omega P_{\text{reac}}(\omega)\simeq-\frac{1}{2}\int_{V_\infty} d^3\mathbf{r}\,[\mu_0|\mathbf{H}_{\text{cl}}|^2+\varepsilon_0\partial_\omega\{\omega\varepsilon_R(\mathbf{r},\omega)\}|\mathbf{E}_{\text{cl}}|^2]$. Consequently, the frequency derivative of the reactive power will be negative, $\partial_\omega P_{\text{reac}}(\omega)<0$, as a manifestation of Foster's reactance theorem [1]. It can be readily checked that $\partial_\omega\triangle\omega(\omega_r)<0$ for such a lossless and nonradiating system. Actually, a similar behavior is expected in most cases since the reactive power is dominated by contributions from the near fields. This implies that taking into account the impact of the reactive power will predict, in most cases, a narrower bandwidth of emission. However, for resonance frequencies ω_r near strongly radiating and/or dissipative points it is possible to observe the reverse behavior, i.e., $\partial_\omega P_{\text{reac}}(\omega)>0$. This outcome in turn leads to a broadening of the bandwidth.

In general, Eq. (19) illustrates that there is an intermediate domain between the usual weak- and strong-coupling regimes where the emission bandwidth can be controlled not only through the decay rate but also through the reactive power. This provides an additional degree of freedom in controlling the bandwidth, which can be used to either broaden or compress it. Thus, it offers new opportunities of engineering the emission spectrum of quantum emitters.

IV. EXAMPLES

The basic theory introduced in the previous section can be applied to a variety of quantum emitters and photonic nanostructures. In the following, we provide some examples illustrating the role of the reactive power in typical configurations of quantum emitters coupled to photonic nanostructures. As we will show, taking into account the role of the reactive power provides a better understanding of the transition from the weak- to the strong-coupling regime, and unveils novel functionalities even in well-studied systems such as resonant cavities and waveguides.

When considering the coupling of a quantum emitter to an inhomogeneous photonic environment, it is convenient to decompose the dyadic Green's function $\mathbf{G}(\mathbf{r},\mathbf{r}',\omega)=\mathbf{G}_{\text{str}}(\mathbf{r},\mathbf{r}',\omega)+\mathbf{G}_0(\mathbf{r},\mathbf{r}',\omega)$ into the addition of a term associated to the modes of a structure of interest $\mathbf{G}_{\text{str}}(\mathbf{r},\mathbf{r}',\omega)$ (e.g., a cavity or a waveguide), as well as a term $\mathbf{G}_0(\mathbf{r},\mathbf{r}',\omega)$ accounting for the rest of the optical modes. Common decompositions include homogeneous and scattering parts [38,39] and cavity and radiating modes [34], although the decomposition into any arbitrary basis is possible. This leads to a similar decomposition for the decay rate, $\Gamma(\omega)=\Gamma_{\text{str}}(\omega)+\Gamma_0$, and frequency shift, $\Delta\omega(\omega)=\Delta\omega_{\text{str}}(\omega)+\Delta\omega_0$. Here, it is typically assumed that the interactions with the modes not of interest are in the weak-coupling regime. This provides a frequency shift that can be included in the emitter's transition frequency $\omega_0+\Delta\omega_0\to\omega_0$ (i.e., the Lamb shift), and an intrinsic decay rate Γ_0 that accounts for all of the radiative decay paths different from the modes of interest. This decay rate can also account for the nonradiative processes intrinsic to the emitter [32–34,40], although a more sophisticated description would be required for nonradiative processes leading to an intrinsic non-Lorentzian spectrum (e.g., emitters with large phonon sidebands).

In this manner, the polarization spectrum can be written as follows:

$$S_0(\omega)=\frac{1}{[\omega-\omega_0-\Delta\omega_{\text{str}}(\omega)]^2+\frac{(\Gamma_{\text{str}}(\omega)+\Gamma_0)^2}{4}}. \tag{21}$$

A. Single-mode cavity: Transition from the weak- to the strong-coupling regime

For illustrative purposes, we start by revisiting the popular example of coupling a quantum emitter with resonance frequency ω_0 to a high-Q single-mode cavity, characterized by the resonant frequency ω_1, linewidth Γ_1, and coupling strength distinguished by the vacuum Rabi frequency Ω_1 [see Fig. 2(a)]. This configuration is a basic textbook example. However, it will serve to illustrate how the proposed intermediate regime describes the transition from the weak- to the strong-coupling regime. First, we note that for a moderate-Q cavity ($\omega_1\gg\Gamma_1$) the decay rate and frequency shift can be approximated by [41] (see also Appendix C)

$$\Delta\omega_{\text{str}}(\omega)-i\frac{\Gamma_{\text{str}}(\omega)}{2}=\frac{\Omega_1^2}{4}\frac{1}{\omega-\omega_1+i\frac{\Gamma_1}{2}}. \tag{22}$$

This model can describe a large number of emitter-cavity configurations. Here, we select parameters typical of a

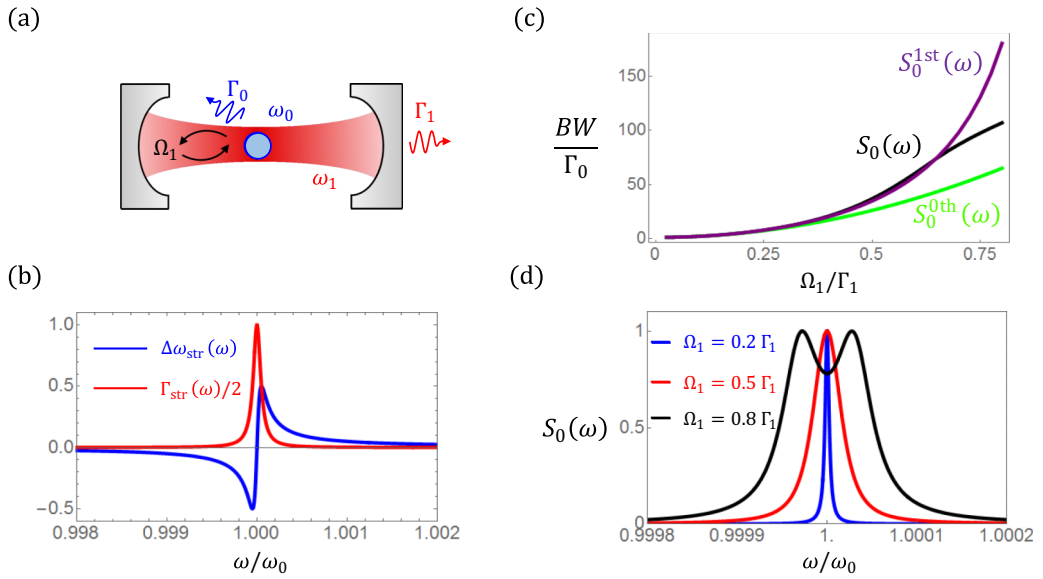

FIG. 2. (a) Sketch of the single-mode cavity geometry: A quantum emitter with transition frequency ω_0 and intrinsic decay rate $\Gamma_0 = 10^{-6}\omega_0$ is coupled to a single-mode cavity with resonance frequency $\omega_1 = \omega_0$, linewidth $\Gamma_1 = 10^{-4}\omega_0$, and coupling strength Ω_1. (b) Dispersive frequency shift $\Delta\omega_{str}(\omega)$ and decay rate $\Gamma_{str}(\omega)$ normalized to their maximum value Ω_1^2/Γ_1. (c) 3-dB emission bandwidth, normalized to the intrinsic decay rate Γ_0, as a function of the normalized coupling strength Ω_1/Γ_1. Comparison between the predictions for the full spectrum $S_0(\omega)$ and zeroth-order $S_0^{0th}(\omega)$ and first-order $S_0^{1st}(\omega)$ approximations. (d) Normalized emission spectrum for coupling strengths $\Omega_1 = 0.2\,\Gamma_1$, $0.5\,\Gamma_1$, and $0.8\,\Gamma_1$.

quantum dot coupled to a photonic crystal cavity, including a moderate-Q resonator with $\Gamma_1 = 10^{-4}\omega_0$, well within the range of known optical cavities (see, e.g., [42]), and an intrinsic linewidth $\Gamma_0 = 10^{-6}\omega_0$ typical of quantum dots (see, e.g., [41], Fig. 5). Coupling strengths Ω_1 enabling the observation of the strong-coupling regime have been reported in a number of experiments (see, e.g., [43]).

Figure 2(b) represents the decay rate $\Gamma_{str}(\omega)$ and frequency shift $\Delta\omega_{str}(\omega)$, confirming that the dispersion is characterized by the Lorentzian line of the cavity. As anticipated, the frequency derivative of the frequency shift is negative at most frequencies, i.e., $\partial_\omega\Delta\omega_{str}(\omega) < 0$. However, this trend is reversed near the resonance: $\omega \sim \omega_0$, where we observe $\partial_\omega\Delta\omega_{str}(\omega) > 0$. Therefore, we can anticipate that as the coupling strength of an emitter tuned to the cavity resonance is increased the bandwidth will tend to be broadened with respect to what could be expected from the zeroth-order approximation (weak-coupling regime) simply by looking at the dispersion of the reactive term $\Delta\omega_{str}(\omega)$. In this manner, considering the impact of the dispersion of the reactive power provides additional insight into the transition from the weak- to the strong-coupling regime.

This point is more clearly illustrated in Fig. 2(c), which depicts the 3-dB bandwidth as a function of the coupling strength. It also compares the bandwidth predicted within the zeroth-order [Eq. (18)] and first-order [Eq. (19)] approximations. For small coupling strengths: $\Omega_1 < 0.3\,\Gamma_1$, the 3-dB bandwidth is correctly predicted by all three formulations. However, for larger coupling strengths, the common zeroth-order approximation provides a pessimistic prediction of the bandwidth, i.e., it fails to account for the broadening induced by the dispersion of the reactive power. Our first-order correction correctly predicts the bandwidth for an extended regime up to roughly $\Omega_1 \sim 0.7\,\Gamma_1$. For larger coupling strengths, the system enters into the strong-coupling regime, and the spectrum is characterized by the well-known two-peaked spectrum usually referred to as Rabi splitting [see Fig. 2(d)].

B. Two-mode cavity: Highly efficient narrow-band source

Next we move to the more interesting question of whether the additional degree of freedom provided by the reactive power can be leveraged to introduce photon sources with novel functionalities. We illustrate this point by analyzing a two-mode resonant cavity and show how this simple structure can be utilized to enable the design of highly efficient narrow-band sources. Typically, the emission efficiency (quantum yield or beta factor) is defined as the ratio between the desired and total decay rates: $\eta = \Gamma_{str}(\omega_0)/[\Gamma_{str}(\omega_0) + \Gamma_0]$ [40]. Usually, efficient photon sources are designed by enhancing the decay rate of the desired channels by means of coupling to photonic nanostructures, i.e., to ensure that $\Gamma_{str}(\omega_0) \gg \Gamma_0$. For this reason, increasing the efficiency is intrinsically associated with bandwidth enlargement. In turn, this feature hinders the design of highly efficient but narrow-band photon sources.

However, highly efficient but narrow-band single-photon sources would be of great interest for a number of applications. For example, bandwidth compression has been shown to help in generating indistinguishable photons, particularly when different physical systems are interfaced [44]. Narrow-band sources are of natural interest for metrology systems, and

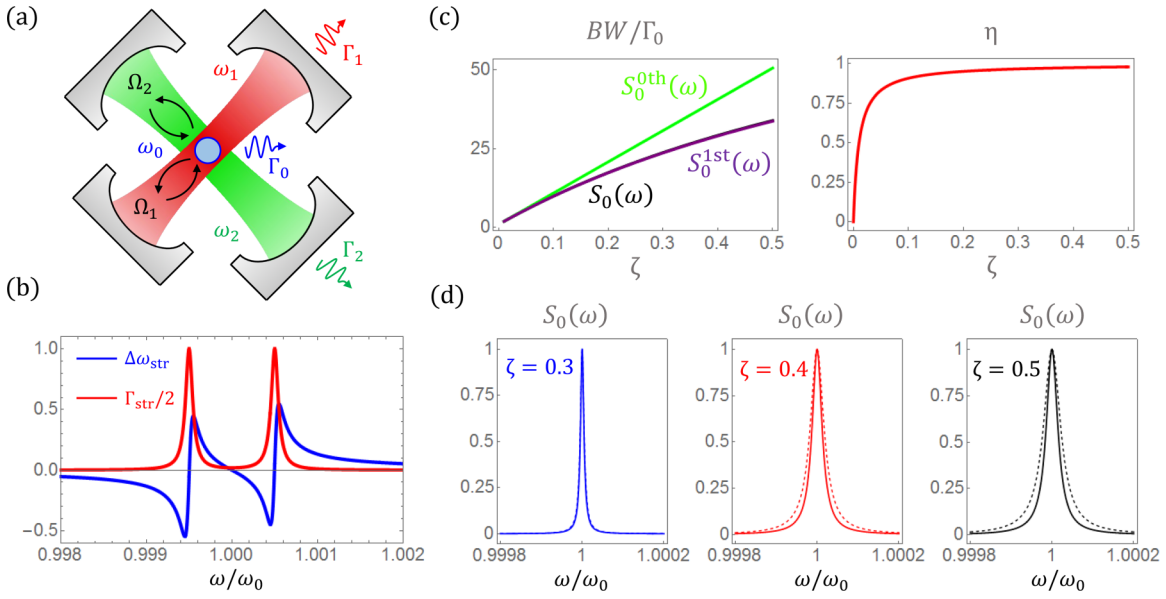

FIG. 3. (a) Sketch of the two-mode cavity geometry: A quantum emitter with transition frequency ω_0 and intrinsic decay rate $\Gamma_0 = 10^{-6}\omega_0$ is coupled to two single-mode cavities the resonance frequencies of which are $\omega_1 = \omega_0 + \omega_\Delta$ and $\omega_0 - \omega_\Delta$. The detuning parameter $\omega_\Delta = 5\,\Gamma_1$, the linewidth $\Gamma_1 = \Gamma_2 = 10^{-4}\omega_0$, and the coupling strength $\Omega_1 = \Omega_2$. (b) Dispersive frequency shift $\Delta\omega_{str}(\omega)$ and decay rate $\Gamma_{str}(\omega)$ normalized to their maximum value Ω_1^2/Γ_1. (c) Comparison between the predictions for the full spectrum $S_0(\omega)$ and zeroth-order $S_0^{0th}(\omega)$ and first-order $S_0^{1st}(\omega)$ approximations. Left: 3-dB emission bandwidth normalized to the intrinsic decay rate Γ_0. Right: Efficiency η as a function of the coupling parameter $\zeta = (\Omega_1/\omega_\Delta)^2/2$. (d) Normalized spectrum for the coupling parameters $\zeta = 0.3$, 0.4, and 0.5. For reference, the zeroth-order approximation is included as a dashed curve.

they would also facilitate spectroscopy with nonclassical light, by interrogating biological or chemical samples with high spectral precision and/or by enhancing the emission from a molecular transition while avoiding the spectral overlap with neighboring transitions. They would also expedite frequency-division multiplexing in quantum communications.

Managing the reactive power can provide a pathway to circumvent the direct relationship between efficiency and narrow-band operation. To illustrate this point, we consider a quantum emitter coupled to a cavity supporting two non-interacting modes (or coupled to two different cavities) as depicted in Fig. 3(a). For the sake of simplicity, we assume that both resonant modes have similar characteristics in terms of coupling strengths, $\Omega_1 = \Omega_2$, and quality factors $\Gamma_1 = \Gamma_2$, but their resonant frequencies are detuned from the transition frequency of the emitter by symmetric shifts $\omega_1 = \omega_0 - \omega_\Delta$ and $\omega_2 = \omega_0 + \omega_\Delta$, respectively. For this configuration, the frequency shift and decay rate can be written as follows:

$$\Delta\omega_{str}(\omega) - i\frac{\Gamma_{str}(\omega)}{2} = \frac{\Omega_1^2}{4}\left(\frac{1}{\omega - \omega_0 + \omega_\Delta + i\frac{\Gamma_1}{2}} + \frac{1}{\omega - \omega_0 - \omega_\Delta + i\frac{\Gamma_1}{2}}\right). \tag{23}$$

The associated dispersion properties of the decay rate and frequency shift are depicted in Fig. 3(b). These results show how the response of the system is characterized by the superposition of two Lorentzian lines, each corresponding to one of the two uncoupled resonant modes. Interestingly, we observe $\Gamma_{str}(\omega_0) \simeq \zeta\,\Gamma_1$, $\Delta\omega_{str}(\omega_0) = 0$, and $\partial_\omega\Delta\omega_{str}(\omega_0) \simeq -\zeta$ at the emitter transition frequency, where we have defined the normalized coupling parameter $\zeta = (\Omega_1/\omega_\Delta)^2/2$. Therefore, this configuration allows for simultaneously enhancing the efficiency by increasing the decay rate, while compressing the bandwidth by the action of the reactive power.

This effect is illustrated in Fig. 3(c), which depicts the 3-dB bandwidth and efficiency of the emitter as functions of the coupling factor ζ. The figure shows that, as the coupling factor increases, the emission bandwidth becomes narrower than the one predicted within the zeroth-order approximation. For example, we have $\eta \simeq 0.98$ at $\zeta = 0.5$, while exhibiting a bandwidth that is 33% smaller than the one predicted purely based on the decay rate. Again, we have used parameter values typical of a quantum dot coupled to a photonic crystal cavity ($\Gamma_1 = 10^{-4}\omega_0$, $\omega_\Delta = 5\,\Gamma_1$, $\Gamma_0 = 10^{-6}\omega_0$). Sweeping the coupling parameter ζ from 0 to 0.5 in this example corresponds to varying the coupling strength Ω_1/Γ_1 from 0 to 5. Values of $\Omega_1/\Gamma_1 = 2.1$ [45], $\Omega_1/\Gamma_1 = 2.7$ [46], and $\Omega_1/\Gamma_1 = 6.4$ [47] have been demonstrated for quantum dots coupled to photonic crystal cavities with similar quality factors.

In this configuration, the first-order correction provides a very accurate prediction of the 3-dB bandwidth for the entire studied parameter range. This effect is justified by the fact that $\partial_\omega^2\Delta\omega_{str}(\omega_0) = 0$, which substantially increases the domain of validity of the first-order correction to the emission spectrum. The normalized spectrum for the coupling parameters $\zeta = 0.3$, 0.4, and 0.5 is reported in Fig. 3(d), which confirms that the spectrum remains Lorentzian but with a bandwidth narrower than the prediction of the

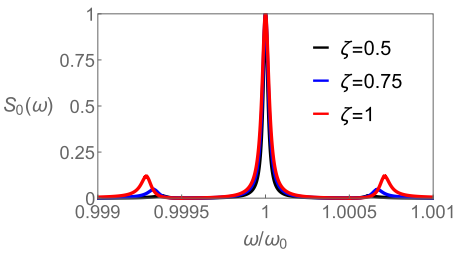

FIG. 4. Normalized emission spectrum for the configuration studied in Fig. 3, but for extended coupling parameters, $\zeta = 0.5$, 0.75, and 1.

zeroth-order approximation (shown as a dashed line). Ultimately, the first-order correction to the emission spectrum will lose its validity when the coupling strength is large enough to enter into the strong-coupling regime, characterized by the presence of multiple emission peaks. This effect is illustrated in Fig. 4, which shows the emission spectrum for an extended range of frequencies and coupling strengths. The figure illustrates how for coupling strengths larger than those studied in Fig. 3 additional peaks would appear in the emission spectrum, signaling the ascension into the strong-coupling regime.

It would be expected that additional functionalities will always come at some cost. In this case, the efficiency achieved for a given cavity system will be smaller than if the emitter was tuned at resonance with the cavity. However, once the quality of the cavity system is high enough so that the efficiency at resonance would become saturated, our results demonstrate that one can achieve a significant bandwidth compression while maintaining a high efficiency. In general, this result sets the basis for the design of highly efficient but narrow-band single-photon sources. Future evolutions of this concept might include many other configurations, for instance, coupled cavities and asymmetric systems, as well as the optimization of the involved parameters, e.g., the quality factors and resonant frequencies of the cavities. These advanced design efforts are beyond the scope of the present investigation.

C. Multimode waveguide: Sub-non-radiative linewidth

The possibility of compressing the bandwidth by managing the reactive power poses the question of how narrow the bandwidth of an initially excited quantum emitter could be theoretically. Typically, one can narrow the bandwidth of a quantum emitter by reducing its decay rate, e.g., by using a closed cavity [48] or a photonic crystal exhibiting a band gap [49,50]. However, both approaches come with the cost of sacrificing efficiency, and, ultimately, this narrowing process stops when the linewidth becomes dominated by nonradiative processes. However, the additional degree of freedom provided by reactive interactions can allow us to circumvent this limit, potentially getting access to sub-non-radiative loss linewidths, even when the emitter is incoherently excited.

We illustrate this possibility by examining a quantum emitter coupled to a multimode waveguide as schematically depicted in Fig. 5(a). For this configuration, the dispersive decay rate and frequency shift can be written as [41,51]

$$\Delta\omega_{\rm str}(\omega) - i\frac{\Gamma_{\rm str}(\omega)}{2} = -i\,\omega \sum_m \alpha_m\, n_{gm}(\omega), \tag{24}$$

where α_m is the coupling parameter to the mth mode. It includes, for instance, the effects of the overlap of the emitter's current distribution with the mode's field profile and its effective volume. The group index of the mth mode is

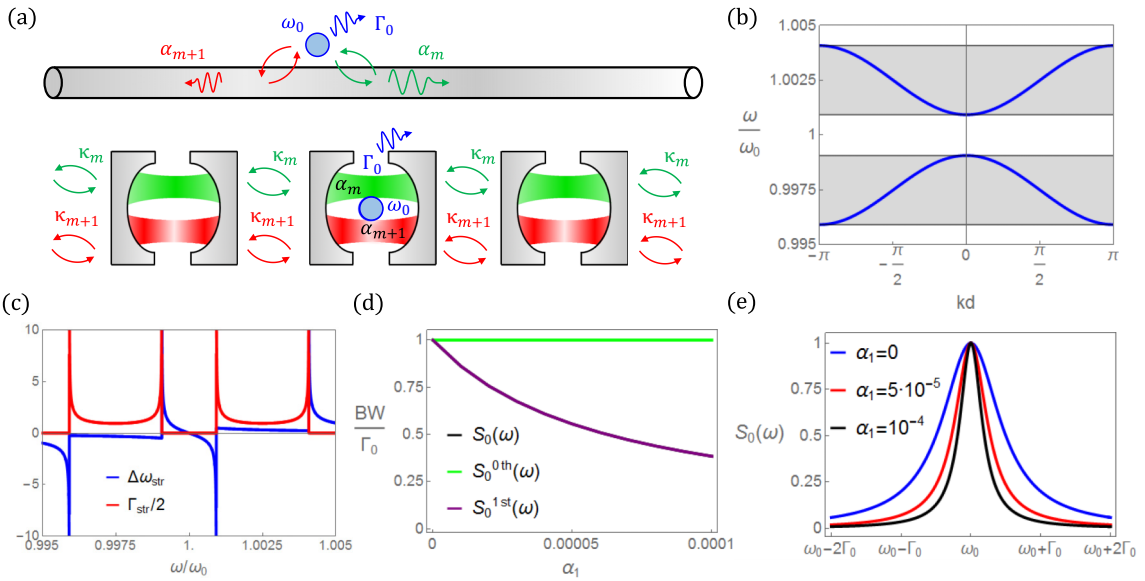

FIG. 5. (a) Sketch of the multimode waveguide geometry: A quantum emitter with transition frequency ω_0 and intrinsic decay rate Γ_0 decays into m modes of a photonic waveguide with coupling factors α_m. Potential implementation is based on a coupled resonator optical waveguide (CROW). (b) Dispersion diagram of the CROW. (c) Dispersive frequency shift $\Delta\omega_{\rm str}(\omega)$ and decay rate $\Gamma_{\rm str}(\omega)$ normalized to its absolute value at the center of the first band $\Gamma_{\rm str}(\omega_1)/2 = \alpha_1\,\omega_1\,n_{g1}(\omega_1)$. (d) 3-dB emission bandwidth normalized to the intrinsic decay rate Γ_0 as a function of the coupling parameter $\alpha_1 = \alpha_2$. (e) Normalized spectrum for the coupling parameters $\alpha_1 = 0$, 0.00005, and 0.0001.

$n_{gm}(\omega) = c/v_{gm}(\omega)$, where $v_{gm}(\omega)$ is the associated group velocity.

It is clear from Eq. (24) that engineering the dispersion properties of the group index $n_{gm}(\omega)$ empowers the design of different light-matter interactions within optical waveguides. To focus our discussion, we consider a coupled resonator optical waveguide (CROW) illustrated in Fig. 5(a) [52,53]. The dispersion relation of a CROW waveguide within the tight-binding approximation can be described as a set of m passbands [52,53] the individual dispersion relations $\omega(k) = \omega_m + \kappa_m \cos(kd)$ of which are centered around the resonance frequencies of the cavity ω_m and the bandwidths of which are equal to two times their coupling rates: $2\kappa_m$. The group index associated with each of these modes is then given by $n_{gm}(\omega) = n_{gm0}/\sqrt{1-(\omega-\omega_m)^2/\kappa_m^2}$, with n_{gm0} being the group index at the center of its passband [54]. We consider the impact of two bands located around the emitter's transition frequency, and set the band parameters to $\omega_1 = 0.9975\,\omega_0$, $\omega_2 = 1.0025\,\omega_0$, $\kappa_1 = \kappa_2 = 0.00158\,\omega_0$, and $n_{gm0} = 15$. Thus, our model matches the band structure and group index reported in CROW waveguide experiments [55] [see Fig. 5(b)].

Figure 5(c) presents the corresponding dispersive frequency shift $\Delta\omega_{\rm str}(\omega)$ and decay rate $\Gamma_{\rm str}(\omega)$. They serve to illustrate some of the salient features of the light-matter interactions within dispersive waveguides. For example, the decay rate is strongly enhanced near the edges of the passbands since it is associated with a large group index, i.e., a near-zero group velocity [41]. Similarly, the medium-assisted Lamb shift is enhanced at the side of the band edge that lies within the band gap [29]. On the other hand, the decay rate is strongly suppressed within the band gaps, leading to an inhibition of the spontaneous emission [49,50] and the formation of long-lived bound states [56–58].

Simultaneously, Fig. 5(c) suggests new opportunities associated with the management of the reactive power within the band gap. For example, we note that if an emitter tuned within the band gap has a nonzero intrinsic decay rate Γ_0 then the dynamics of the quantum emitter would still be dominated by an exponential relaxation through the channels external to the waveguide system. This feature is true even if $\Gamma_{\rm str}(\omega_0) = 0$. In such a case, the emission spectrum would be expected to be a Lorentzian line with a 3-dB bandwidth Γ_0. However, at the center of the band gap, we have $\Delta\omega_{\rm str}(\omega) = 0$ and a negative frequency derivative $\partial_\omega \Delta\omega_{\rm str}(\omega) < 0$. These are the necessary ingredients for bandwidth compression beyond that induced by an inhibition of spontaneous emission. This effect is shown in Figs. 5(d) and 5(e) in which the quantum emitter 3-dB bandwidth and emission spectrum are depicted as functions of the coupling parameter $\alpha_1 = \alpha_2$. As expected, the bandwidth is identical to the intrinsic decay rate Γ_0 for small coupling parameters $\alpha_1 \sim 0$. On the other hand, it is compressed beyond this limit as the coupling parameter strengthens and the zeroth-order approximation is no longer valid. This bandwidth compression effect is found to monotonically increase along with the coupling. However, the first-order corrections will lose their validity for large coupling parameters, i.e., as the system enters into the strong-coupling regime and additional emission peaks appear (see Fig. 4). Again, different parameters of the system, e.g., the separation and width of the propagating bands, could be optimized to achieve a better performance for specific waveguide implementations and/or particular applications. Other structures exhibiting a band gap, such as photonic crystal [59] and metamaterial [60,61] waveguides, could also be considered.

In general, these results demonstrate the real possibility of using a photonic nanostructure to compress the bandwidth of a quantum emitter beyond the limit of its nonradiative linewidth. It is worth remarking that the so-called subnatural linewidth photon emission based on resonance fluorescence operating in Heitler's regime has been reported [62–64]. However, recent theoretical developments indicate that subnatural linewidth and antibunching cannot be observed simultaneously in this configuration unless the coherent part of the emitted light is reduced by destructive interference with an external coherent signal [65]. The operating principle of our configuration is entirely different. First, since it is not based on resonance fluorescence, it does not involve the illumination of the emitter with a continuous-wave laser. Consequently, it does not require the exact compensation of different terms in order to guarantee antibunching. Second, our proposed system is consistent with incoherent pumping and is thus compatible with electronically driven devices. In fact, if the intrinsic decay rate Γ_0 is dominated by a radiative component (outside the waveguide system), our system would allow for on-demand operation. Finally, achieving an intrinsic line narrower than the width associated with the nonradiative losses might have important implications in the dynamics of different decoherence channels beyond manipulating the emission bandwidths of quantum emitters.

V. CONCLUSIONS

Our results demonstrate that reactive interactions can be exploited as an additional degree of freedom in controlling the bandwidth of quantum emitters. This degree of freedom can be used either in the compression or in the expansion of the bandwidth, while maintaining a Lorentzian spectrum. Being able to control the bandwidth of emission beyond the manipulation of its decay rate provides a finer control and offers new possibilities. For instance, it is possible to elude a direct relationship between the bandwidth and efficiency. This feature facilitates the design of efficient quantum emitters preserving a narrow bandwidth. It also enables the compression of the source's bandwidth beyond limits imposed by nonradiative decay rates intrinsic to the emitter. We have outlined the basic theory and presented examples associated with applications involving resonant cavities and waveguides. This basic theory and these configurations could be implemented through a variety of systems, including different quantum emitters (cold atoms, ions, quantum dots, color centers, etc.), multiple emitters, resonant cavities (defect cavity modes in photonic crystals, nanopillar cavities, whispering gallery modes, plasmonic cavities, etc.), and/or photonic crystal and metamaterial waveguides. Many other configurations, e.g., coupled cavities, nanoparticle systems, and waveguides with different dispersion profiles, could also be explored. In general, our results take inspiration from classic antenna theory to provide a perspective on the interactions of quantum emitters with their photonic environments. Moreover, they may find

important applications in the development of nonclassical light sources.

ACKNOWLEDGMENTS

I.L. acknowledges support from a Juan de la Cierva Incorporación Fellowship and from an additional grant from Caixa.

APPENDIX A: IMPACT OF THE DISPERSION OF THE DECAY RATE IN THE EMISSION SPECTRUM

This paper mainly focuses on studying the impact of reactive interactions on the bandwidth of quantum emitters. However, for the sake of completeness, here we discuss the impact of the dispersion of the decay rate on the emission spectrum. To this end, a first-order correction to the emission spectrum, including the impact of the dispersion of the decay rate, can be found by approximating $\Delta\omega(\omega) \simeq \Delta\omega(\omega_r)$ and $\Gamma(\omega) \simeq \Gamma(\omega_r) + \partial_\omega\Gamma(\omega_r)(\omega - \omega_r)$, around the resonance frequency, and leading to

$$S^{\text{first}}_{0,\Gamma}(\omega) = \frac{1}{(\omega-\omega_r)^2 + \frac{\Gamma^2(\omega_r)}{4}[1 + C_\Gamma(\omega-\omega_r)]}, \tag{A1}$$

with $C_\Gamma = 2\partial_\omega\Gamma(\omega_r)/\Gamma(\omega_r)$. It is clear from Eq. (A1) that this correction introduces an additional term proportional to $(\omega - \omega_r)$, which changes sign around ω_r. Therefore, we conclude that the first-order effect of the dispersion of the decay rate is inducing an asymmetry on the Lorentzian line.

If we simultaneously consider a first-order correction of both the decay rate and the frequency shift, the spectrum can be written as follows:

$$S^{\text{first}}_{0,\Gamma,\Delta\omega} = \frac{1}{C_\Delta^2}\frac{1}{(\omega-\omega_r)^2 + \frac{\Gamma^2(\omega_r)}{4C_\Delta^2}[1 + C_\Gamma(\omega-\omega_r)]}, \tag{A2}$$

with the definition $C_\Delta = 1 - \partial_\omega\Delta\omega(\omega_r)$. It can be concluded from Eq. (A2) that the resulting spectrum will again be an asymmetric line. However, the overall width of this asymmetric line will then be controlled by the dispersion of the frequency shift (reactive interactions) via the C_Δ parameter. Therefore, we expect that our findings could be extended even to configurations where the dispersion of the decay rate cannot be neglected.

APPENDIX B: DISPERSION PROPERTIES OF THE REACTIVE POWER: DERIVATION OF EQ. (20)

In this Appendix we provide the derivation of Eq. (20) of the main text, i.e., an expression of the frequency derivative of the reactive power in terms of field quantities. To this end, we adapt previous results of antenna theory [1,4] to our case with a fixed current distribution. Our starting point is the time-harmonic Maxwell curl equations for the classical electric and magnetic vector fields

$$\nabla \times \mathbf{E}(\mathbf{r},\omega) = i\omega\mu_0\mathbf{H}(\mathbf{r},\omega), \tag{B1}$$

$$\nabla \times \mathbf{H}(\mathbf{r},\omega) = -i\omega\epsilon_0\epsilon(\mathbf{r},\omega)\mathbf{E}(\mathbf{r},\omega) + \mathbf{j}(\mathbf{r}) \tag{B2}$$

and their frequency derivatives

$$\nabla \times \partial_\omega\mathbf{E}(\mathbf{r},\omega) = i\mu_0\mathbf{H}(\mathbf{r},\omega) + i\omega\mu_0\partial_\omega\mathbf{H}(\mathbf{r},\omega), \tag{B3}$$

$$\nabla \times \partial_\omega\mathbf{H}(\mathbf{r},\omega) = -i\epsilon_0\partial_\omega\{\omega\epsilon(\mathbf{r},\omega)\}\mathbf{E}(\mathbf{r},\omega) - i\omega\epsilon_0\epsilon(\mathbf{r},\omega)\partial_\omega\mathbf{E}(\mathbf{r},\omega). \tag{B4}$$

The explicit spatial and frequency dependencies of the field and permittivity quantities are omitted hereafter to alleviate the notation. Next, we construct a variation of Poynting's theorem by substracting $\nabla\cdot(\partial_\omega\mathbf{E}\times\mathbf{H}^*)$ and $\nabla\cdot(\mathbf{E}\times\partial_\omega\mathbf{H}^*)$, and taking the imaginary part, so that we can write

$$\begin{aligned}&\text{Im}\nabla\cdot(\partial_\omega\mathbf{E}\times\mathbf{H}^* - \mathbf{E}\times\partial_\omega\mathbf{H}^*)\\ &= -\text{Im}\{\mathbf{j}^*\cdot\partial_\omega\mathbf{E}\} + \mu_0|\mathbf{H}|^2 + \epsilon_0\partial_\omega\{\omega\epsilon_R\}|\mathbf{E}|^2\\ &\quad -2\omega\epsilon_0\epsilon_I\text{Im}\{\partial_\omega\mathbf{E}^*\cdot\mathbf{E}\}.\end{aligned} \tag{B5}$$

In this manner, we can compute the frequency derivative of the reactive power by integrating (B5) over an asymptotically large volume V_∞ bounded by the surface S_∞:

$$\begin{aligned}\partial_\omega P_{\text{reac}}(\omega) &= -\frac{1}{2}\int_{V_\infty} d^3\mathbf{r}\ \ \text{Im}\{\mathbf{j}^*\cdot\partial_\omega\mathbf{E}\}\\ &= -\frac{1}{2}\int_{V_\infty} d^3\mathbf{r}[\mu_0|\mathbf{H}|^2 + \epsilon_0\partial_\omega\{\omega\epsilon_R\}|\mathbf{E}|^2]\\ &\quad + \omega\epsilon_0\int_{V_\infty} d^3\mathbf{r}\,\epsilon_I\,\text{Im}\{\partial_\omega\mathbf{E}^*\cdot\mathbf{E}\}\\ &\quad + \frac{1}{2}\text{Im}\oint_{S_\infty} d\mathbf{S}\cdot(\partial_\omega\mathbf{E}\times\mathbf{H}^* - \mathbf{E}\times\partial_\omega\mathbf{H}^*).\end{aligned} \tag{B6}$$

We simplify the last term by noting that the surface integral is taken in the far zone of the sources $\mathbf{j}(\mathbf{r})$. Therefore, we can write the following limits for the electric and magnetic fields:

$$\lim_{r\to\infty}\mathbf{E} = \frac{e^{i\frac{\omega}{c}r}}{r}\mathbf{F}(\mathbf{u}_r), \tag{B7}$$

$$\lim_{r\to\infty}\mathbf{H} = \frac{1}{\eta_0}\frac{e^{i\frac{\omega}{c}r}}{r}\mathbf{u}_r\times\mathbf{F}(\mathbf{u}_r), \tag{B8}$$

where $\mathbf{F}(\mathbf{u}_r)$ is the emission pattern in the far zone, and for their frequency derivatives

$$\lim_{r\to\infty}\partial_\omega\mathbf{E} = \frac{i}{c}\mathbf{F}(\mathbf{u}_r)\,e^{i\frac{\omega}{c}r}, \tag{B9}$$

$$\lim_{r\to\infty}\partial_\omega\mathbf{H} = \frac{i}{c}\frac{1}{\eta_0}\mathbf{u}_r\times\mathbf{F}(\mathbf{u}_r)\,e^{i\frac{\omega}{c}r}. \tag{B10}$$

By using these limits, the last term in (B6) reduces to

$$\begin{aligned}&\frac{1}{2}\text{Im}\oint_{S_\infty} d\mathbf{S}\cdot(\partial_\omega\mathbf{E}\times\mathbf{H}^* - \mathbf{E}\times\partial_\omega\mathbf{H}^*)\\ &= \mu_0\oint_{S_\infty} d\Omega\, r|\mathbf{F}(\mathbf{u}_r)|^2.\end{aligned} \tag{B11}$$

Finally, introducing (B11) into (B6), one recovers Eq. (20) of the main text.

APPENDIX C: HIGH QUALITY FACTOR APPROXIMATION FOR THE INTERACTION WITH A SINGLE-MODE CAVITY

Here we provide additional details on the expression used to model the interaction energy term for a quantum emitter coupled to a single-mode cavity, i.e., Eq. (22) of the main text. In particular, we consider a single-mode cavity with resonant frequency ω_1, decay rate Γ_1, and normalized mode function $\mathbf{u}_1(\mathbf{r})$. The dyadic Green's function of this system can be written as follows [41]:

$$\mathbf{G}(\mathbf{r},\mathbf{r}',\omega) = -\omega^2 \frac{\mathbf{u}_1(\mathbf{r})\mathbf{u}_1^*(\mathbf{r}')}{\omega^2-\omega_1^2+i\omega\Gamma_1}. \tag{C1}$$

This expression is commonly used to model the interaction between a quantum emitter and a single-mode cavity. However, a simpler but very accurate expression can be obtained by taking the narrow-band approximation: $\omega^2-\omega_1^2+i\omega\Gamma_1 \simeq 2(\omega-\omega_1+i\Gamma_1/2)$ in the denominator and $\omega^2 \simeq \omega_1^2$ in the numerator. In this manner, the dyadic Green's function reduces to

$$\mathbf{G}(\mathbf{r},\mathbf{r}',\omega) \simeq -\frac{\omega_1^2}{2}\frac{\mathbf{u}_1(\mathbf{r})\mathbf{u}_1^*(\mathbf{r}')}{\omega-\omega_1+i\frac{\Gamma_1}{2}}. \tag{C2}$$

Consequently, following the definition of the dispersive frequency shift and decay rate in Eq. (14), we find

$$\triangle\omega(\omega) - i\frac{\Gamma(\omega)}{2} = \frac{1}{\omega-\omega_1+i\frac{\Gamma_1}{2}}\frac{\mu_0\omega_1^2}{2\hbar}\left|\int d^3\mathbf{r}\ \mathbf{j}_{\mathrm{ge}}^*(\mathbf{r})\cdot\mathbf{u}_1(\mathbf{r})\right|^2, \tag{C3}$$

which is identical to the expression used in the main text, with the definition of the coupling strength:

$$\Omega_1^2 = \frac{2\mu_0\omega_1^2}{\hbar}\left|\int d^3\mathbf{r}\ \mathbf{j}_{\mathrm{ge}}^*(\mathbf{r})\cdot\mathbf{u}_1(\mathbf{r})\right|^2. \tag{C4}$$

We remark that this approximation is extremely accurate even for cavities with much smaller Γ_1/ω_1 ratios than those considered in the paper.

[1] R. Harrington, *Time-Harmonic Electromagnetic Fields* (McGraw-Hill, New York, 1961).
[2] C. A. Balanis, *Advanced Engineering Electromagnetics* (Wiley, New York, 1999).
[3] K. Schab, L. Jelinek, M. Capek, C. Ehrenborg, D. Tayli, G. A. Vandenbosch, and M. Gustafsson, IEEE Access **6**, 10553 (2018).
[4] A. D. Yaghjian and S. R. Best, IEEE Trans. Antennas Propag. **53**, 1298 (2005).
[5] H. A. Wheeler, Proc. IRE **35**, 1479 (1947).
[6] L. J. Chu, J. Appl. Phys. **19**, 1163 (1948).
[7] R. F. Harrington, J. Res. Nat. Bur. Stand. **64D**, 1 (1960).
[8] R. Collin and S. Rothschild, IEEE Trans. Antennas Propag. **12**, 23 (1964).
[9] R. Fante, IEEE Trans. Antennas Propag. **17**, 151 (1969).
[10] J. S. McLean, IEEE Trans. Antennas Propag. **44**, 672 (1996).
[11] H. L. Thal, IEEE Trans. Antennas Propag. **54**, 2757 (2006).
[12] M. Gustafsson, C. Sohl, and G. Kristensson, Proc. R. Soc. A **463**, 2589 (2007).
[13] A. D. Yaghjian and H. R. Stuart, IEEE Trans. Antennas Propag. **58**, 3114 (2010).
[14] G. A. Vandenbosch, IEEE Trans. Antennas Propag. **59**, 2217 (2011).
[15] O. S. Kim, IEEE Trans. Antennas Propag. **64**, 146 (2016).
[16] J. L. Volakis, C.-C. Chen, and K. Fujimoto, *Small Antennas: Miniaturization Techniques and Applications* (McGraw-Hill, New York, 2010).
[17] S. R. Best, IEEE Trans. Antennas Propag. **52**, 953 (2004).
[18] R. Ziolkowski and A. Erentok, IET Microwaves, Antennas Propag. **1**, 116 (2007).
[19] P. Jin and R. W. Ziolkowski, IEEE Trans. Antennas Propag. **57**, 2548 (2009).
[20] O. S. Kim, IEEE Trans. Antennas Propag. **58**, 2210 (2010).
[21] M. Gustafsson and S. Nordebo, IEEE Trans. Antennas Propag. **61**, 1109 (2013).
[22] M. Gustafsson, D. Tayli, C. Ehrenborg, M. Cismasu, and S. Nordebo, FERMAT **15**, 1 (2016).
[23] L. Jelinek and M. Capek, IEEE Trans. Antennas Propag. **65**, 329 (2017).
[24] M. Scully, A. Sokolov, and A. Svidzinsky, Opt. Photon. News **29**, 34 (2018).
[25] W. E. Lamb and R. C. Retherford, Phys. Rev. **72**, 241 (1947).
[26] M. O. Scully, Phys. Rev. Lett. **102**, 143601 (2009).
[27] R. Röhlsberger, K. Schlage, B. Sahoo, S. Couet, and R. Rüffer, Science **328**, 1248 (2010).
[28] P. Yao, C. Van Vlack, A. Reza, M. Patterson, M. M. Dignam, and S. Hughes, Phys. Rev. B **80**, 195106 (2009).
[29] R. Sokhoyan and H. A. Atwater, Opt. Express **21**, 32279 (2013).
[30] I. Liberal and N. Engheta, Sci. Adv. **2**, e1600987 (2016).
[31] S. Haroche and J.-M. Raimond, *Exploring the Quantum: Atoms, Cavities, and Photons* (Oxford University, New York, 2006).
[32] A. Delga, J. Feist, J. Bravo-Abad, and F. J. Garcia-Vidal, Phys. Rev. Lett. **112**, 253601 (2014).
[33] C. Van Vlack, P. T. Kristensen, and S. Hughes, Phy. Rev. B **85**, 075303 (2012).
[34] S. Hughes and P. Yao, Opt. Express **17**, 3322 (2009).
[35] W. Vogel and D.-G. Welsch, *Quantum Optics* (Wiley, New York, 2006).
[36] M. Wubs, L. G. Suttorp, and A. Lagendijk, Phys. Rev. A **70**, 053823 (2004).
[37] J. Binney and D. Skinner, *The Physics of Quantum Mechanics* (Oxford University, New York, 2013).
[38] S. Scheel, L. Knöll, and D.-G. Welsch, Phys. Rev. A **60**, 4094 (1999).
[39] H. T. Dung, L. Knöll, and D.-G. Welsch, Phys. Rev. A **62**, 053804 (2000).
[40] L. Novotny and B. Hecht, *Principles of Nano-Optics* (Cambridge University, Cambridge, England, 2012).
[41] P. Lodahl, S. Mahmoodian, and S. Stobbe, Rev. Modern Phys. **87**, 347 (2015).
[42] K. J. Vahala, Nature (London) **424**, 839 (2003).

[43] T. Yoshie, A. Scherer, J. Hendrickson, G. Khitrova, H. Gibbs, G. Rupper, C. Ell, O. Shchekin, and D. Deppe, Nature (London) **432**, 200 (2004).
[44] M. Karpiński, M. Jachura, L. J. Wright, and B. J. Smith, Nature Photon. **11**, 53 (2017).
[45] R. Ohta, Y. Ota, M. Nomura, N. Kumagai, S. Ishida, S. Iwamoto, and Y. Arakawa, Appl. Phys. Lett. **98**, 173104 (2011).
[46] T. Volz, A. Reinhard, M. Winger, A. Badolato, K. J. Hennessy, E. L. Hu, and A. Imamoğlu, Nat. Photonics **6**, 605 (2012).
[47] Y. Ota, D. Takamiya, R. Ohta, H. Takagi, N. Kumagai, S. Iwamoto, and Y. Arakawa, Appl. Phys. Lett. **112**, 093101 (2018).
[48] D. Kleppner, Phys. Rev. Lett. **47**, 233 (1981).
[49] V. P. Bykov, Sov. J. Quantum Electron. **4**, 861 (1975).
[50] E. Yablonovitch, Phys. Rev. Lett. **58**, 2059 (1987).
[51] S. Hughes, Opt. Lett. **29**, 2659 (2004).
[52] A. Yariv, Y. Xu, R. K. Lee, and A. Scherer, Opt. Lett. **24**, 711 (1999).
[53] J. K. Poon, J. Scheuer, Y. Xu, and A. Yariv, J. Opt. Soc. Am. B **21**, 1665 (2004).
[54] A. Martínez, A. García, P. Sanchis, and J. Martí, J. Opt. Soc. Am. A **20**, 147 (2003).
[55] M. L. Cooper, G. Gupta, M. A. Schneider, W. M. Green, S. Assefa, F. Xia, Y. A. Vlasov, and S. Mookherjea, Opt. Express **18**, 26505 (2010).
[56] S. John and J. Wang, Phys. Rev. Lett. **64**, 2418 (1990).
[57] G. Calajó, F. Ciccarello, D. Chang, and P. Rabl, Phys. Rev. A **93**, 033833 (2016).
[58] T. Shi, Y.-H. Wu, A. González-Tudela, and J. I. Cirac, Phys. Rev. X **6**, 021027 (2016).
[59] J. D. Joannopoulos, S. G. Johnson, J. N. Winn, and R. D. Meade, *Photonic Crystals: Molding the Flow of Light* (Princeton University, Princeton, NJ, 2011).
[60] C. Caloz and T. Itoh, *Electromagnetic Metamaterials: Transmission Line Theory and Microwave Applications* (Wiley, New York, 2005).
[61] G. V. Eleftheriades and K. G. Balmain, *Negative-Refraction Metamaterials: Fundamental Principles and Applications* (Wiley, New York, 2005).
[62] W. Heitler, *The Quantum Theory of Radiation* (Oxford University, New York, 1954).
[63] H.-S. Nguyen, G. Sallen, C. Voisin, P. Roussignol, C. Diederichs, and G. Cassabois, Appl. Phys. Lett. **99**, 261904 (2011).
[64] C. Matthiesen, A. N. Vamivakas, and M. Atatüre, Phys. Rev. Lett. **108**, 093602 (2012).
[65] J. C. L. Carreño, E. Z. Casalengua, F. P. Laussy, and E. del Valle, Quantum Sci. Technol. **3**, 045001 (2018).